Optical Materials: X 13 (2022) 100135

Contents lists available at ScienceDirect

Optical Materials: X

journal homepage: www.journals.elsevier.com/optical-materials-x

Invited Article

(INVITED) Opto-electronic properties of solution-synthesized MoS_2 metal-semiconductor-metal photodetector

Omar A. Abbas [1], Chung-Che Huang, Daniel W. Hewak, Sakellaris Mailis [1], Pier Sazio *

Optoelectronics Research Centre, University of Southampton, Southampton, SO17 1BJ, United Kingdom

ARTICLE INFO

Keywords:
MSM photodetector
MoS_2
Schottky contacts

ABSTRACT

We report a simple fabrication method for metal-semiconductor-metal (MSM) photodetectors using solution-synthesized MoS_2 films as the semiconductor channel and pure indium for the metal contacts. Resonance Raman spectroscopy has been used to confirm the growth of ultra-thin MoS_2 films. Due to the low work function of indium, the back-to-back indium-MoS_2 Schottky junctions formed relatively low Schottky barrier height (0.43 eV), which has been calculated using the thermionic field emission model. Moreover, the MSM device shows good responsivity (22 mA/W) under white light illumination. The MoS_2-MSM device possesses higher photo-electrical response in the visible and near IR region compared to UV due to the indirect bandgap of ultra-thin MoS_2 film which has been estimated to be 1.38 eV. These findings reveal the significance of using low work function metals like indium as contacts for layered transition metal dichalcogenides (TMDC) films (produced by low cost solution-based techniques), particularly MoS_2, in order to design semiconductor devices with efficient opto-electronic performance.

1. Introduction

Two-dimensional materials have stirred rapidly growing interest after the discovery of graphene due to their diverse properties that can be exploited in wide range of applications [1]. An interesting subcategory from this broad materials group are the two-dimensional transition metal dichalcogenides (2D-TMDC), which are layered semiconducting materials that predominantly exhibit 1–2 eV electronic bandgap [2]. Moreover, their bandgap can be modified by composition, which enables tailoring the spectral responsivity of TMD based photodetectors. For example, in MoS_2 by just substituting sulphur with tellurium, to obtain $MoTe_2$, the operational range shifts from the visible to the infrared region [2].

MoS_2 is a widely researched 2D-TMDC due to its natural abundance [3], thickness-dependent bandgap [4,5] and excellent electrical [6]/photoelectrical [7] behaviour, therefore, there has been significant progress in the realisation of next-generation MoS_2 electronics [8], optoelectronics [3] and photonics [9] devices.

One of the significant challenges related to these materials that needs to be addressed is determining a suitable production strategy to be adopted by industry [2]. Several methods have been proposed for MoS_2 synthesis, for example: chemical vapour deposition (CVD) [10], pulsed laser deposition (PLD) [11] and sputtering [2]. For industrial purposes, thermolysis of single source precursor films like ammonium tetrathiomolybdate $(NH_4)_2MoS_4$ constitutes a very promising approach, where meter-scale continuous roll to roll MoS_2 films with excellent thickness and composition homogeneity can be produced [12].

Another crucial challenge facing 2D materials and in particular MoS_2, that needs special consideration is the metal contact engineering, as it is an essential step to design and fabricate electronic and opto-electronic devices with high performance, low power consumption and fast response [13]. Platinum, gold, tungsten, nickel, aluminium, titanium and scandium have all been investigated for metallisation of single crystalline MoS_2 flakes (exfoliated from natural bulk crystals) where they show diverse electrical junction properties and output currents ranging from Schottky to Ohmic, depending on their work functions [14,15].

Indium is a soft metal with low work-function and is mature in terms of integration with semiconductor technology. Very recently, indium was deposited using electron-beam and thermal evaporation processes on MoS_2 resulting a successful formation of Ohmic-like Van der Waals junctions with low contact resistance [16,17]. However, it has been

* Corresponding author.
E-mail address: pjas@soton.ac.uk (P. Sazio).
[1] **Present address:** Skolkovo Institute of Science and Technology Novaya St., 100, Skolkovo 143025, Russian Federation.

https://doi.org/10.1016/j.omx.2022.100135
Received 17 February 2021; Received in revised form 30 December 2021; Accepted 3 January 2022
Available online 12 January 2022

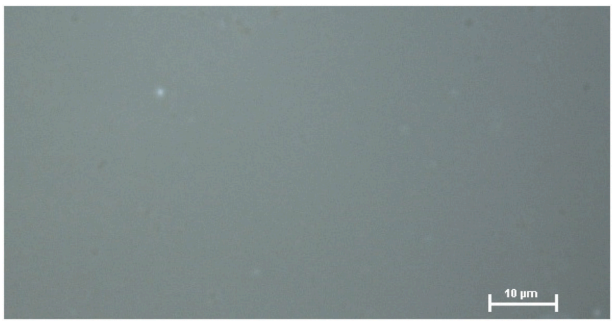

Fig. 1. Optical microscope image of spin coated 31 mg $(NH_4)_2MoS_4$ solution dissolved in 5 mL (24 mM) solvent mixture with ratio (2: DMF, 2: n-butylamine and 1:2-aminoethanol) over oxygen plasma treated silica substrate. The substrate was pre-annealed at 90 °C for 5 min to evaporate the solvents.

reported by Liu et al., that the chemical alteration resulting from metal evaporation and metal left-off processes is one of the aggravation factors for fermi level pining in metal-semiconductor interfaces, resulting in a high deviation from the Schottky–Mott model which describes ideally the behaviour of charge carrier in metal-semiconductor junctions [18].

In this paper, the electronic and optoelectronic properties of back-to-back indium-ultra thin MoS_2 films Schottky junctions have been investigated in a metal-semiconductor-metal (MSM) photodetector device. The solution-synthesized MoS_2 films were grown by two-step thermolysis of spin-coated ammonium tetrathiomolybdate films at high temperatures. We fabricated the contacts by simply stacking scalpel-cut Indium slivers directly on the MoS_2 films to exclude any metal evaporation or lithographic steps. The I–V characteristics of the MoS_2-MSM device under dark conditions have been investigated and the main parameters such as ideality factor, reverse saturation current and Schottky barrier height have been extracted. Moreover, the MoS_2-MSM device shows excellent responsivity under white light illumination due to the broad spectral photoelectrical response of the device ranging from NIR to UV regions. The work presented here investigates the electronic and optoelectronic behaviour of low Schottky barrier height junctions formed between semiconducting ultra-thin MoS_2 films and the two Indium contacts.

2. Experimental methods

2.1. Preparation of $(NH_4)_2MoS_4$ solutions and substrates for growth of MoS_2 films

The initial step to produce MoS_2 films by thermolysis of ammonium tetrathiomolybdate $(NH_4)_2MoS_4$ is to coat the targeted substrates with the precursor solution. The chemistry of the precursor solution and hydrophilicity of substrate surface are vital to deposit highly uniform and defect-free precursor layers, especially when spin-coating technique is applied, as these will be thermally decomposed via annealing to produce highly uniform MoS_2 films.

To prepare the precursor solution, 31 mg of $(NH_4)_2MoS_4$ has been dissolved in 5 mL solvent system to create 24 mM precursor solution (where the solvent system contains 2 mL: dimethylformamide (DMF), 2 mL: n-butylamine and 1 mL:2-aminoethanol). The solutions were sonicated for 15–20 min to improve the solubility and homogeneity. This solvents recipe has been adopted from Yang et al., with modifications on the solvents ratios to preserve the uniformity of the precursor layer [19].

In addition to the solvent recipe, substrate conditioning plays an important role to avoid clusters and pinholes formation on the coated substrate, thus allowing the homogeneous formation of films. It has been shown by Yang et al., that a few seconds of oxygen plasma etching improves the wettability of the $(NH_4)_2MoS_4$ solution on the substrates [19]. However, we found it was more suitable and reproducible if all the substrates were exposed to oxygen plasma etching with the following details: 1000 W power, 10 min exposure time, oxygen flow rate1000 mL/min and 0.1 mbar pressure. It is worth noting that prior to plasma treatments, the substrates were all cleaned sequentially by acetone, isopropanol, methanol and deionized water then dried using nitrogen flow.

Finally, the $(NH_4)_2MoS_4$ solutions were spin-cast for 1 min as the following: Step 1- ramp 5 s, dwell time 5 s, rpm 500; Step 2- ramp 5 s, dwell time 45 s, 3000 rpm. Prior to annealing, the samples were pre-baked in ambient conditions directly after spin-coating for 1–5 min at 90 °C to solidify the precursor layer. Fig. 1 is an optical microscopic image that shows spin-coated $(NH_4)_2MoS_4$ film on silica substrate deposited by the aforementioned procedure.

2.2. Thermal decomposition and device fabrication

The samples consisted of spin-coated $(NH_4)_2MoS_4$ films (formed by 24 mM solution concentration) on 1.5 cm^2 SiO_2/Si substrates with 300 nm oxide layer were placed inside a tube furnace for the thermal decomposition step. During the 20-min ramping time of furnace, the samples were kept in the cold zone under 1 mbar pressure and 100 sccm purge flow of (6% H_2/Ar). Once the furnace temperature reached 500 °C, the samples were repositioned to the hot zone for 30 min annealing at this temperature. After the first annealing step, the samples were left to cool down naturally while maintaining the flow of gas. Normally, the MoS_2 films grown by thermal decomposition at 500 °C suffer from short-range crystalline order, hence, they exhibit poor electrical and optical properties [20]. Crystallinity enhancement for MoS_2 films was therefore implemented by a second annealing step at 1000 °C in Ar environment with 100 sccm flow under atmospheric pressure for 15 min. The samples were exposed to the targeted temperature after the furnace levelled-off and once the annealing step finished (15 min), the samples were moved out of the hot zone to cool down naturally to room temperature. To preserve the composition of MoS_2 films at the high temperature, we performed the processing using a face to face arrangement of identical

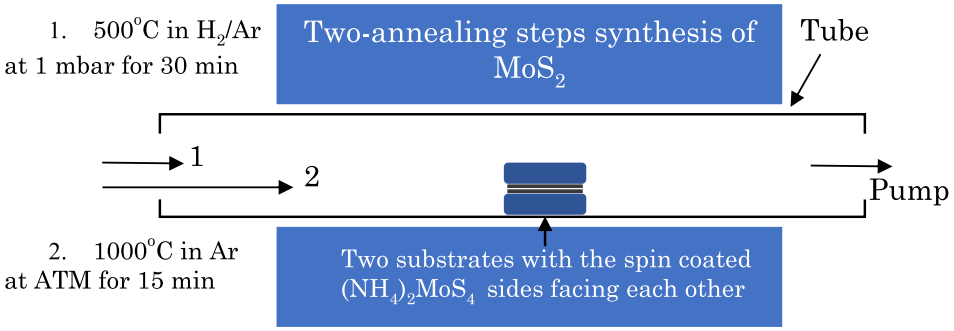

Fig. 2. Schematic diagram for the furnace system that was used for the synthesis of MoS_2 via two-step thermal decomposition/annealing of $(NH_4)_2MoS_4$.

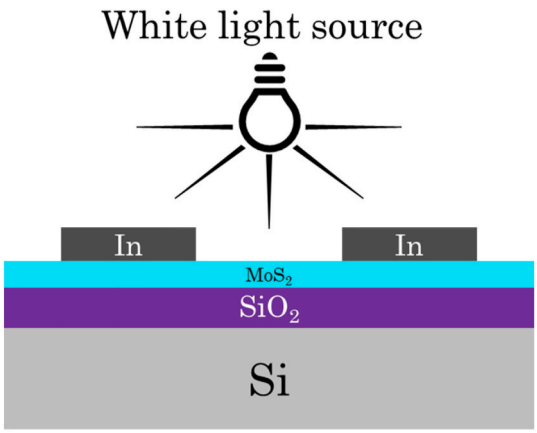

Fig. 3. Schematic diagram of MoS_2-MSM device.

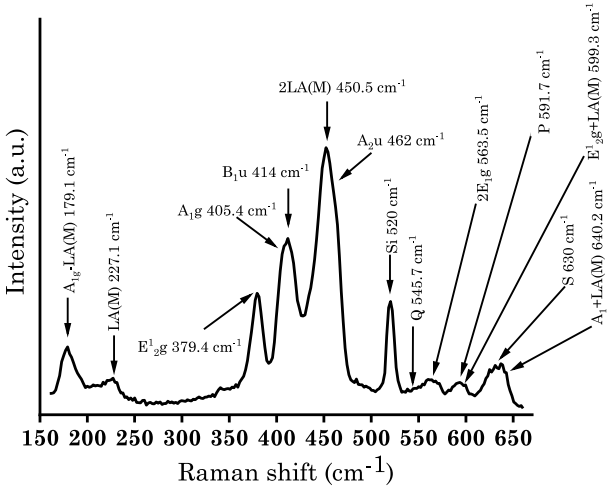

Fig. 4. Raman spectra of MoS_2 films grown by thermolysis of spin-coated ammonium tetrathiomolybdate with 24 mM concentration.

sample pairs as shown in Fig. 2.

In order to investigate the rectifying and photodetection properties of the MoS_2 films with indium contacts, a metal-semiconductor-metal device was fabricated. The metallisation process is as follows: two indium metal slivers were cut and pressed gently on the MoS_2 film; the contacts conformed well to the surface of the sample as indium is a soft metal. The spacing between the two contacts was about 3 mm long and 3 mm wide. Prior to the metallisation step, the indium contacts were etched using 10% hydrochloric acid solution diluted in di-ionized water to remove the native oxide from the surface, which can degrade the performance of the contacts. Fig. 3 shows a schematic diagram for MoS_2 metal-semiconductor-metal (MSM) photodetector device.

3. Results and discussion

3.1. Raman spectroscopy of MoS_2

In order to confirm the growth of semiconductor MoS_2 films, Raman spectroscopy has been conducted with excitation wavelength of 633 nm and 20 mW power using 50X objective. Fig. 4 shows the Raman spectra of MoS_2 films grown by thermolysis of spin-coated ammonium tetrathiomolybdate films using 24 mM concentration. It is worth mentioning that Lorentzian fitting was used to obtain the peaks' positions and all peaks are labelled according to Refs. [21,22]. The Raman characteristic peaks for MoS_2 are E2g and A1g which are centred at 379.4 cm^{-1} and 405.4 cm^{-1} respectively, with a wavenumber difference (A1g- E2g) of 26 cm^{-1}.

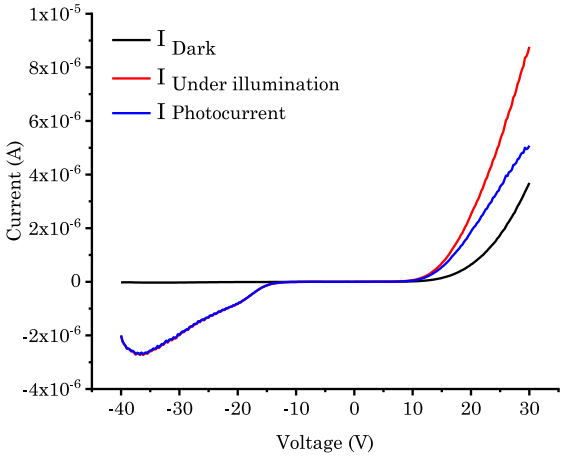

Fig. 5. Linear graph of I–V characteristics of MoS_2 MSM photodetector where the black line represents the dark current (without illumination), the red line represents the current under white light illumination and the blue line is the net photocurrent.

Additional Raman peaks, as compared to spectra corresponding to shorter wavelength excitation lasers [21], appear through the whole scanning range of energies as shown in Fig. 4. The existence of these second-order Raman peaks is due to the resonance of excitation wavelength (633 nm) with the direct band gap of MoS_2 [21,22]. In addition to the application of Raman spectroscopy for MoS_2 growth verification, it is also used to estimate the number of MoS_2 layers [21,22].

It should be noted that the positions and the separation of Raman characteristic peaks (A1g- E2g = 26 cm^{-1}) [22], the prominence of LA (M) peak at 227.1 cm^{-1}, which does not appear in bulk MoS_2 [22] and the broadening of MoS_2 peaks at wavenumbers between 530 cm^{-1} to 650 cm^{-1}, that leads to split additional peaks (Q,P and S), which are not found bulk MoS_2 [22] are sufficient evidence that the MoS_2 films are ultra-thin in nature.

3.2. Extraction of dark and photocurrent parameters of multi-layered MoS_2 MSM photodiode

It is well known that the electrical behaviour of metal-semiconductor junctions has either Ohmic or Schottky nature, and the Schottky barrier, which represents the difference between the work function of the metal contact and the electron affinity of the semiconductor can be estimated according to Schottky–Mott rule [18]:-

$$\Phi_{SB} = \Phi_{metal} - \chi \qquad \text{equation 1}$$

where Φ_{SB} is the Schottky barrier for electrons and Φ_{metal} is the work function of the metal and χ represents the electron affinity of the semiconductor. Indium has a low work function (4.12 eV) [23–26] while the electron affinity of multi-layered MoS_2 is about 4 eV [14,15,27,28]. This means indium contact with MoS_2 has a Schottky barrier of just 0.12 eV. However, this Schottky barrier is theoretical and it could be significantly different when a real device is fabricated.

Fig. 5 depicts the current-voltage characteristics of In–MoS_2–In (metal-semiconductor-metal) device under dark conditions (black line) and white light illumination (red line). The device shows a rectifying behaviour when the voltage is swept forward from −40 V to 40 V (the graph is limited to 30 V), the large area of the semiconductor channel (MoS_2) enables the device to work on relatively high voltages without voltage breakdown in reverse bias. This indicates that the MoS_2 film synthesized by our method is semiconducting whereas the Schottky barrier is higher than what was predicted in the equation above as the

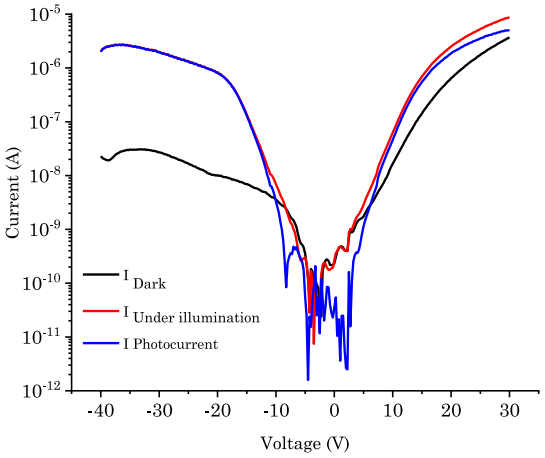

Fig. 6. Log-Linear graph of I–V characteristics of MoS_2 MSM photodetector where the black line represents the dark current (without illumination), the red line represents the current under white light illumination and the blue line is the photocurrent induced by light.

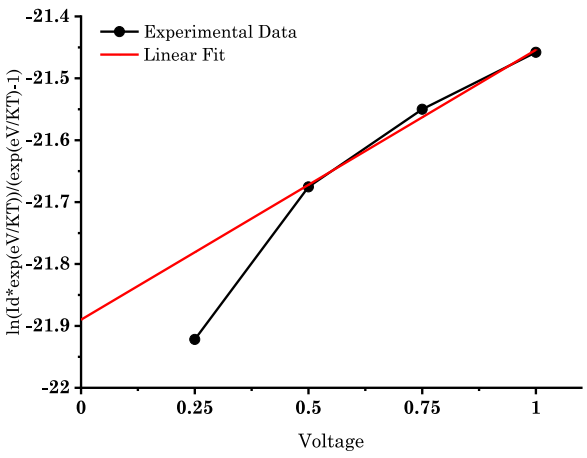

Fig. 7. ln ((I exp (eV/KT))/(exp (eV/KT)-1)) as a function of forward voltage. The black dotted line represents the actual data while the red line is the linear fit which its intersection with y-axis represents ln I_o. Note: data at 0.25 V has been excluded from the extrapolation as it is the nonlinear part of the Ln function.

rectifying behaviour is unidirectional.

One of the main diode parameters is the rectifying ratio, which is defined as the ratio of the forward current to the reverse saturation current when the same magnitude of voltage is applied for both directions (forward and reverse bias) in dark condition [29]. The rectifying ratio has been calculated to be 4.09×10^2 at −40 and 40 V for the (In–MoS_2–In) device. Moreover, the turn-on voltage for the diode has been extrapolated from the tangent of the exponential part for the dark current (black line in Fig. 5) when intersects the x-axis and it is found to be 24 V.

Generally, the current through the Schottky diode (for bulk semiconductors like silicon or gallium arsenide) in both forward and reverse bias can be expressed by thermionic emission mechanism where the carriers (electrons or holes) overcome the Schottky barrier when they have sufficient thermal energy. This mechanism can be expressed using the expression [30]:-

$$I = I_o\left[\exp\left(\frac{eV}{KT}\right) - 1\right] \qquad \text{equation 2}$$

where I is the current flowing through the diode, e is the electron charge 1.6×10^{-19} Coulombs, K is Boltzmann constant 1.38×10^{-23} m^2 kg s^{-2} K^{-1}, T is the temperature in Kelvin (298 K for room temperature) and Io is the reverse saturation current which can be expressed as below [30]:-

$$I_o = AA^*T^2 exp\left(-\frac{e\Phi_{SB}}{KT}\right) \qquad \text{equation 3}$$

where A is the area of the diode in cm^2, A^* is Richardson constant for the semiconductor material, T is the temperature in Kelvin, e is the electron charge, K is Boltzmann constant and Φ_{SB} is the Schottky barrier in eV.

However, the thermionic emission model is only valid when the reverse saturation current is totally levelled off in reverse bias (i.e. independent of the reverse voltage bias) and the ideality factor (which is a number that measures how close the actual device behaves to an ideal diode) is equal to 1 [30,31].

The semi-log graph for I–V characteristics in Fig. 6 shows that the reverse saturation current of our device is reverse bias dependent. In other words, the reverse saturation current increases as applied reverse voltage increases. Furthermore, the device configuration consisted of two back-to-back Schottky diodes meaning that the ideality factor is much higher than one.

This means thermionic emission is not the main mechanism that can be attributed to the rectifying behaviour of our device. Tunnelling, diffusion or both are the dominant carrier transport mechanisms in the metal-semiconductor interface [31,32]. In this case, the thermionic-field emission model could be more appropriate to analyse the rectifying behaviour of our device. The equation below describes the thermionic-field emission model [30]:-

$$I = I_o\left\{exp\left(\frac{eV}{nKT}\right) - exp\left[\frac{\left(\frac{1}{n} - 1\right)eV}{KT}\right]\right\} \qquad \text{equation 4}$$

where all the parameters are mentioned previously and n is the ideality factor, knowing that when n is equal to 1, Equation (4) is simplified to be Equation (2) again. Now, in order to extract the parameters such as the reverse saturation current and the ideality factor, Equation (4) could be rearranged to be [33]:-

$$\frac{I\exp\left(\frac{eV}{KT}\right)}{\exp\left(\frac{eV}{KT}\right) - 1} = I_o\exp\left(\frac{eV}{nKT}\right) \qquad \text{equation 5}$$

If the natural logarithm is taken for the both sides, Equation (5) will be:

$$\ln\left(\frac{I\exp\left(\frac{eV}{KT}\right)}{\exp\left(\frac{eV}{KT}\right) - 1}\right) = \ln I_o + \frac{eV}{nKT} \qquad \text{equation 6}$$

where the left-hand side of Equation (6) can be plotted as a function of the forward voltage (see Fig. 7) which I, V, e, K and T are known. To find reverse saturation current Io, the linear extrapolation has been implemented for the actual data from 0.5 to 1 volt in forward bias where the y-intersect represents ln Io. It is worth noting that data at 0.25 V has been excluded from the extrapolation as it is the nonlinear part of the Ln function. The reason behind taking a small forward voltage range is to avoid the series resistance effect of the diode [34]. The reverse saturation current is 3.11×10^{-10} A.

Moreover, to extract the ideality factor as function of the forward voltage. Equation (6) should be derived and rearranged to be [33]:-

$$n(V) = \frac{e}{KT}\frac{dV}{d\ln\left[\frac{I\ exp\ (eV/KT)}{exp\ (eV/KT) - 1}\right]} \qquad \text{equation 7}$$

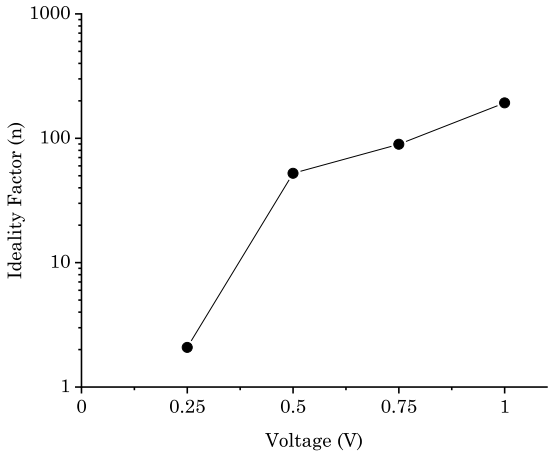

Fig. 8. Semi-log plot of ideality factor as function of the forward voltage. As it is clear the ideality factor was close to 2 only at very small voltage and increased significantly as the voltage increased due to the series resistance of the device.

The plot of the ideality factor as a function of the voltage is shown in Fig. 8. The ideality factor at 0.25 V is 2, which is close to organic and GaAs devices [31]. However, the ideality factor increases rapidly with voltage due to the effect of the series resistance of the device, large active area as well as the double Schottky contacts configuration [35].

Another important parameter for the diode is the Schottky barrier, which can be calculated from equation (3) as the saturation current has been obtained previously. Knowing that the Richardson constant for MoS_2 is 0.70 $\times$ 10^{-6} A cm^{-2} K^{-2} [36], the Schottky barrier for indium-MoS_2-indium interfaces is 0.43 eV. This value is almost identical with computational prediction of the Schottky barrier height of an indium-MoS_2 interface [37].

To study the photoresponse of indium-MoS_2-indium MSM photodiode, the device was illuminated by an incandescent white light source with intensity 1 mW/cm^2 while the source drain voltage was being swept from −40 V to 30 V. As shown in Fig. 5, the reverse saturation current under illumination (red line) has been improved dramatically as compared to the dark current one, which indicates a photocurrent was generated due to the photoconductive nature of the MoS_2 film (blue line). The photocurrent has been calculated and plotted by subtraction of the dark current from the current under illumination ($I_{photocurrent} = I_{under\ illumination} - I_{dark}$) [38], as shown in Figs. 5 and 6 respectively. The contrast ratio, which is photo-to-dark current ratio ($I_{photocurrent}/I_{dark}$) [39,40] has been calculated to be 96.1 at −40 V. An important opto-electronic figure of merit is the responsivity where it is defined as the ratio of the photocurrent to the optical power of this incident light as expressed below [38]:-

$$R = \frac{Photocurrent(I_{ph})}{Input\ \ optical\ \ Power(P_{in})} \qquad \text{equation 8}$$

where the input optical power calculated by multiplying the illuminating intensity (1 mW/cm^{-2}) with the channel area (0.09 cm^{-2}) while the photocurrent is 2.018 $\times$ 10^{-6} A at −40 V. The responsivity of the device is 0.022 AW^{-1} at −40 V, which is comparable to what was reported earlier for few-layer MoS_2-MSM device [41].

3.3. Dark and photocurrent generation mechanism in MoS_2 -MSM photodetector

The rectifying and photodetection parameters were extracted from the data. These parameters aid the understanding of the rise of the dark current and photocurrent in our MSM multi-layered MoS_2 device. However, in order to have clear idea about the mechanism of current generation, the energy band diagrams were used to visualize the whole

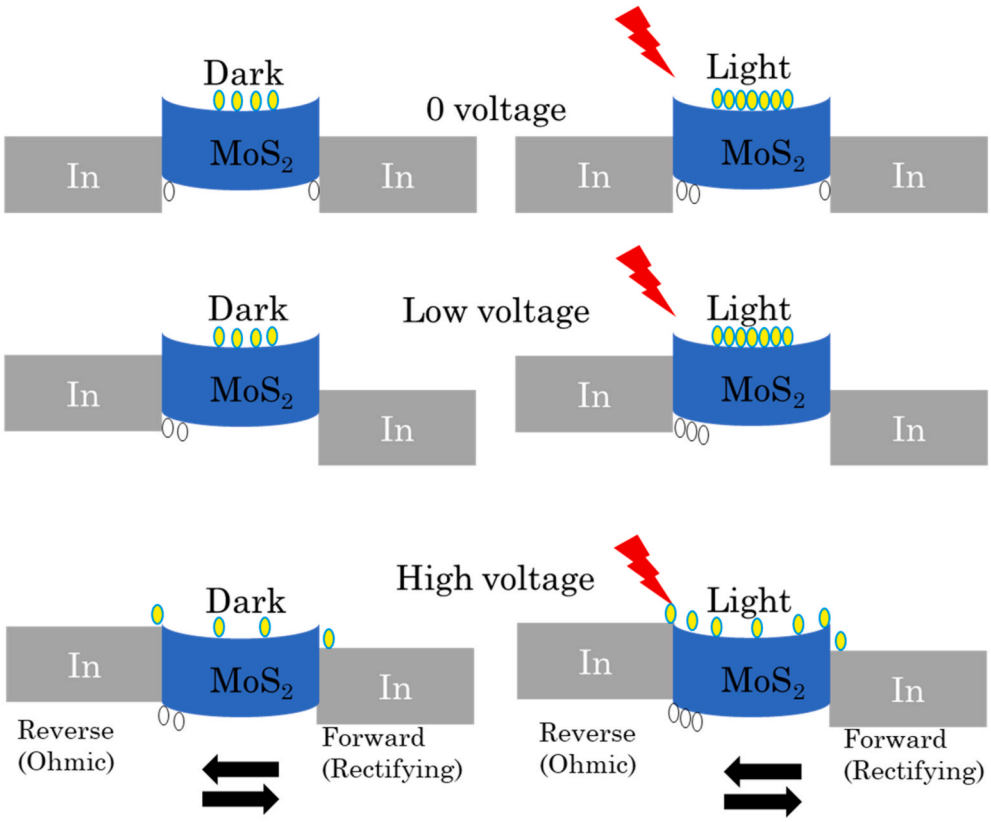

Fig. 9. Schematics illustrates the conduction mechanism of MoS_2 MSM photodiode under dark and white light illumination.

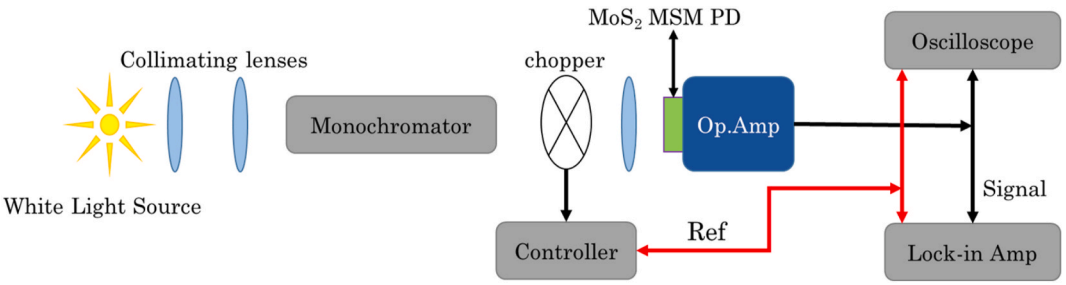

Fig. 10. Schematic diagram of spectral response measurement experimental set up used for MoS_2 MSM device.

process as shown in Fig. 9. According to this model, the current generation process is divided into three parts based on the biasing regimes: zero voltage (equilibrium), low voltage and high voltage.

In principle, metal-semiconductor-metal photodiode are two Schottky diodes, which are connected back to back via the semiconductor channel [42]. At equilibrium, when there is no external voltage applied at dark conditions, no current will pass through or be generated by the MoS_2-MSM device in any direction as the net built-in electric field for both Schottky junctions is equal to zero [43]. Under illumination, the light excites (generates) electrons-hole pairs while the Schottky barriers are still high and there is no biasing voltage to overcome the barrier potentials. Consequently, the majority carriers (electrons for solution based MoS_2 as suggested by the literature [20]) in the conduction band are trapped between the two Schottky barriers as they tend to repel from the metal-semiconductor potential barriers due to the built-in electric field [43–45]. On the contrary, the minority carriers (holes) generated by traps and defects are attracted to the metal-semiconductor interfaces driven by the same built-in electric fields [43–45]. Although, carrier concentration increases dramatically due to photoexcitation, the net photocurrent at zero voltage is also zero as the carriers are trapped between the two electrodes and there is no possible path to extract them [45]. It is worth mentioning that a photocurrent can be generated if the contacts of the photodiode are asymmetrical, for example when one of the contact is Schottky and the other one is Ohmic [46], or even if the area of the two Schottky contacts is not identical [45]. Under these conditions, the MSM photodetector could work in the photovoltaic regime and photocurrent can flow without the need for external bias.

At low biasing voltage, the Schottky barriers will be lowered. However, at low voltages the current flow through the two junctions is mainly attributed to thermionic emission in both dark and illuminated conditions. Therefore, the electron injection from one Schottky junction can pass smoothly through one junction but it will be repressed due to reverse bias in the second Schottky junction, (which increases the height of the barrier). As a result, the output current for both contacts will be limited by the saturation current of the back-to-back diode connections [47], which is voltage and light power independent in this case. In our device the low voltage range is from -8 V to 4 V, as shown previously in Fig. 6, where there is no significant difference between the current in dark and illuminated conditions as well as very low conductivity for both scenarios as the main conduction mechanism is attributed to reverse thermionic current.

At higher voltages, the tunnelling starts to dominate the current flow and the high external applied voltage reduces the Schottky barriers for both junctions. However, the minority carriers (holes) generated by traps or defects in the valence band that are trapped at the interface of the metal-semiconductor start to accumulate and begin crowding in the negative potential junction (reverse bias) rather than the positive one (forward bias). This flattens the Schottky barrier in reverse bias to become more Ohmic-like, leading to semi linear (Ohmic) behaviour on the negative side.

Under reverse bias, the dark current becomes voltage dependent and increases with the bias voltage (see Fig. 6). When the device is illuminated, the majority carrier density increases significantly due to photoexcitation while the minority carriers (holes) from traps or defects tend to modify the Schottky barrier to become more Ohmic. Finally, the photocurrent will increase and the device will behave as a photoconductor.

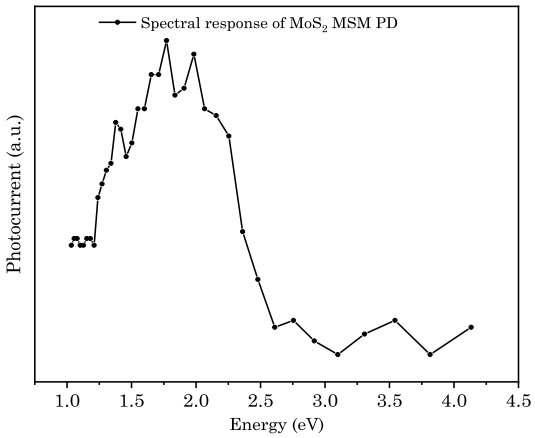

Fig. 11. Spectral response of MoS_2 MSM photodiode from near IR to near UV spectrum.

However, at high forward bias, lowering of Schottky barrier is only due to the external voltage, while there is no contribution from the minority carriers (holes) from traps or defects to modify the barrier, which leads to a small Schottky barrier formation under high forward bias. The current passing through the Schottky junction under high forward bias has an exponential dependence on the voltage as illustrated in Fig. 6. When the device is illuminated, electron injection is improved, leading to a reduction of the "turn on" voltage and the dynamic resistance of the device as shown in Fig. 6.

To sum up, the In–MoS_2–In device behaves as two back-to-back Schottky junctions at equilibrium (0 volt) and low bias with no output current at zero volts and only reverse saturation current being observed for low voltage. Once high voltage is applied, the device behaves as a single In–MoS_2 Schottky junction with bias-dependent saturation current, thus, we analyse it as a single device with thermionic-field emission model (see equation (4)). Under illumination, asymmetrical I–V characteristics are more obvious (see Figs. 6 and 7).

3.4. Spectral response of MoS_2 MSM device

Spectral response measurement (photocurrent or responsivity as a function of the wavelength) is a technique used to study the sensitivity of the detector for each specific photon energy (wavelength) to estimate the operational bandwidth of the device. Fig. 10 shows a diagram for the experimental set up of spectral response measurement (photocurrent spectroscopy).

The spectral response of the photocurrent, which was measured

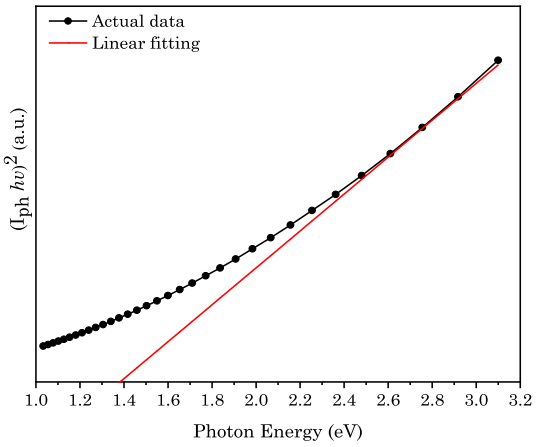

Fig. 12. Plot of (Iph$h\upsilon$) ^{2} vs photon energy (eV), the dotted black line represents the actual data while the solid red line is the tangent of the curve where its intersection with photon energy axis is the bandgap of the MoS_2 device [48].

within the range of 300 nm–1200 nm (1–4.1 eV) is depicted in Fig. 11. The device shows higher responsivity in visible and near infrared region as compared to the near UV. There are two noticeable peaks in the spectrum where the current induced by photons increases rapidly which are located at 1.77 eV and 1.98 eV. According to the literature, the enhanced photocurrent at these photon energies can be associated with the A and B exciton absorption peaks respectively [4,5]. Another advantage of spectral measurement is that the electronic band gap of transition metal dichalcogenides could be estimated using spectral response of the photocurrent using Tauc extrapolation technique [48,49]. Assuming the optical and electronic band gaps are identical in inorganic TMD materials means that the photocurrent is proportional to the absorption coefficient near the absorption edge of the bandgap [48,49]. To further confirm the band structure of MoS_2 film, a Tauc curve has been plotted with respect to photon energy and $(I_{ph}h\upsilon)^2$ based on the relationship below [48]:-

$$\left(I_{ph}h\upsilon\right)^2 \propto \left(h\upsilon - E_g^{Opt}\right) \qquad \text{equation 9}$$

where the absorption coefficient is substituted by the photocurrent as they both have a proportional relation [48,49]. Fig. 12 represents the relation above and the linear extrapolation and intercept of this curve with the photon energy axis gives an estimated (indirect) band gap of 1.382 eV. As was mentioned earlier the band gap is thickness dependent in MoS_2. This value of the bandgap is with good agreement for few-layer MoS_2 [5].

4. Conclusions

A facile method for the fabrication of a few-layer MoS_2 MSM device, based on solution-based single source precursor has been demonstrated. Electrical characterisation of the In–MoS_2–In MSM shows the formation of a low Schottky barrier height (0.43 eV) due to the low work function of Indium which boosts the electrical performance of the device. Benefiting from low Schottky barrier, the photoelectrical responsivity under white light illumination of the MoS_2-MSM was measured to be relatively high (22 mA/W). Our results highlight the advantages of using Indium as a metal contact for MoS_2 films for future electronic and optoelectronic MoS_2-based devices.

CRediT authorship contribution statement

Omar A. Abbas: Conceptualization, Methodology, Investigation, Data curation, Writing – original draft, Visualization. **Chung-Che Huang:** Resources. **Daniel W. Hewak:** Supervision, Project administration, Funding acquisition. **Sakellaris Mailis:** Supervision, Project administration, Funding acquisition, Writing – review & editing. **Pier Sazio:** Supervision, Project administration, Funding acquisition, Writing – review & editing.

Declaration of competing interest

The authors declare that they have no known competing financial interests or personal relationships that could have appeared to influence the work reported in this paper.

Acknowledgements

The first author gratefully acknowledges the financial support from The Higher Committee for Education Development in Iraq (HCED Iraq). The authors acknowledge financial support from the UK's Engineering and Physical Sciences Research Council (EPSRC) through National Hub in High Value Photonic Manufacturing (grant No. EP/N00762X/1) and Russian Science Foundation (RSF) (grant No. 21-79-20208). We also thank Dr. Adam H. Lewis for performing Raman spectroscopy.

References

[1] A.C. Ferrari, F. Bonaccorso, V. Fal'ko, K.S. Novoselov, S. Roche, P. Bøggild, S. Borini, F.H.L. Koppens, V. Palermo, N. Pugno, J.A. Garrido, R. Sordan, A. Bianco, L. Ballerini, M. Prato, E. Lidorikis, J. Kivioja, C. Marinelli, T. Ryhänen, A. Morpurgo, J.N. Coleman, V. Nicolosi, L. Colombo, A. Fert, M. Garcia-Hernandez, A. Bachtold, G.F. Schneider, F. Guinea, C. Dekker, M. Barbone, Z. Sun, C. Galiotis, A.N. Grigorenko, G. Konstantatos, A. Kis, M. Katsnelson, L. Vandersypen, A. Loiseau, V. Morandi, D. Neumaier, E. Treossi, V. Pellegrini, M. Polini, A. Tredicucci, G.M. Williams, B. Hee Hong, J.H. Ahn, J. Min Kim, H. Zirath, B. J. Van Wees, H. Van Der Zant, L. Occhipinti, A. Di Matteo, I.A. Kinloch, T. Seyller, E. Quesnel, X. Feng, K. Teo, N. Rupesinghe, P. Hakonen, S.R.T. Neil, Q. Tannock, T. Löfwander, J. Kinaret, Science and technology roadmap for graphene, related two-dimensional crystals, and hybrid systems, Nanoscale 7 (2015) 4598–4810, https://doi.org/10.1039/c4nr01600a.

[2] M. Samadi, N. Sarikhani, M. Zirak, H. Zhang, H.L. Zhang, A.Z. Moshfegh, Group 6 transition metal dichalcogenide nanomaterials: synthesis, applications and future perspectives, Nanoscale Horiz. 3 (2018) 90–204, https://doi.org/10.1039/c7nh00137a.

[3] Q.H. Wang, K. Kalantar-Zadeh, A. Kis, J.N. Coleman, M.S. Strano, Electronics and optoelectronics of two-dimensional transition metal dichalcogenides, Nat. Nanotechnol. 7 (2012) 699–712, https://doi.org/10.1038/nnano.2012.193.

[4] A. Splendiani, L. Sun, Y. Zhang, T. Li, J. Kim, C.Y. Chim, G. Galli, F. Wang, Emerging photoluminescence in monolayer MoS_2, Nano Lett. 10 (2010) 1271–1275, https://doi.org/10.1021/nl903868w.

[5] K.F. Mak, C. Lee, J. Hone, J. Shan, T.F. Heinz, Atomically thin MoS_2: a new direct-gap semiconductor, Phys. Rev. Lett. 105 (2010) 136805, https://doi.org/10.1103/PhysRevLett.105.136805.

[6] B. Radisavljevic, A. Radenovic, J. Brivio, V. Giacometti, A. Kis, Single-layer MoS_2 transistors, Nat. Nanotechnol. 6 (2011) 147–150, https://doi.org/10.1038/nnano.2010.279.

[7] Z. Yin, H. Li, H. Li, L. Jiang, Y. Shi, Y. Sun, G. Lu, Q. Zhang, X. Chen, H. Zhang, Single-layer MoS_2 phototransistors, ACS Nano 6 (2012) 74–80, https://doi.org/10.1021/nn2024557.

[8] D. Lembke, S. Bertolazzi, A. Kis, Single-layer MoS_2 electronics, Acc. Chem. Res. 48 (2015) 100–110, https://doi.org/10.1021/ar500274q.

[9] K.F. Mak, J. Shan, Photonics and optoelectronics of 2D semiconductor transition metal dichalcogenides, Nat. Photonics 10 (2016) 216–226, https://doi.org/10.1038/nphoton.2015.282.

[10] Y. Zhang, Y. Yao, M.G. Sendeku, L. Yin, X. Zhan, F. Wang, Z. Wang, J. He, Recent progress in CVD growth of 2D transition metal dichalcogenides and related heterostructures, Adv. Mater. 31 (2019) 1901694, https://doi.org/10.1002/adma.201901694.

[11] Z. Yang, J. Hao, Progress in pulsed laser deposited two-dimensional layered materials for device applications, J. Mater. Chem. C. 4 (2016) 8859–8878, https://doi.org/10.1039/c6tc01602b.

[12] Y.R. Lim, J.K. Han, S.K. Kim, Y.B. Lee, Y. Yoon, S.J. Kim, B.K. Min, Y. Kim, C. Jeon, S. Won, J.H. Kim, W. Song, S. Myung, S.S. Lee, K.S. An, J. Lim, Roll-to-Roll production of layer-controlled molybdenum disulfide: a platform for 2D semiconductor-based industrial applications, Adv. Mater. 30 (2018) 1705270, https://doi.org/10.1002/adma.201705270.

[13] A. Allain, J. Kang, K. Banerjee, A. Kis, Electrical contacts to two-dimensional semiconductors, Nat. Mater. 14 (2015) 1195–1205, https://doi.org/10.1038/nmat4452.

[14] S. Walia, S. Balendhran, Y. Wang, R. Ab Kadir, A. Sabirin Zoolfakar, P. Atkin, J. Zhen Ou, S. Sriram, K. Kalantar-Zadeh, M. Bhaskaran, Characterization of metal contacts for two-dimensional MoS_2 nanoflakes, Appl. Phys. Lett. 103 (2013) 232105, https://doi.org/10.1063/1.4840317.

[15] S. Das, H.Y. Chen, A.V. Penumatcha, J. Appenzeller, High performance multilayer MoS_2 transistors with scandium contacts, Nano Lett. 13 (2013) 100–105, https://doi.org/10.1021/nl303583v.
[16] Y. Wang, J.C. Kim, R.J. Wu, J. Martinez, X. Song, J. Yang, F. Zhao, A. Mkhoyan, H. Y. Jeong, M. Chhowalla, Van der Waals contacts between three-dimensional metals and two-dimensional semiconductors, Nature 568 (2019) 70–74, https://doi.org/10.1038/s41586-019-1052-3.
[17] B.K. Kim, T.H. Kim, D.H. Choi, H. Kim, K. Watanabe, T. Taniguchi, H. Rho, J. J. Kim, Y.H. Kim, M.H. Bae, Origins of genuine Ohmic van der Waals contact between indium and MoS_2, Npj 2D Mater. Appl. 5 (2021) 1–9, https://doi.org/10.1038/s41699-020-00191-z.
[18] Y. Liu, J. Guo, E. Zhu, L. Liao, S.J. Lee, M. Ding, I. Shakir, V. Gambin, Y. Huang, X. Duan, Approaching the Schottky-Mott limit in van der Waals metal-semiconductor junctions, Nature 557 (2018) 696–700, https://doi.org/10.1038/s41586-018-0129-8.
[19] J. Yang, Y. Gu, E. Lee, H. Lee, S.H. Park, M.H. Cho, Y.H. Kim, Y.H. Kim, H. Kim, Wafer-scale synthesis of thickness-controllable MoS_2 films via solution-processing using a dimethylformamide/n-butylamine/2-aminoethanol solvent system, Nanoscale 7 (2015) 9311–9319, https://doi.org/10.1039/c5nr01486g.
[20] K.-K. Liu, W. Zhang, Y.-H. Lee, Y.-C. Lin, M.-T. Chang, C.-Y. Su, C.-S. Chang, H. Li, Y. Shi, H. Zhang, C.-S. Lai, L.-J. Li, Growth of large-area and highly crystalline MoS_2 thin layers on insulating substrates, Nano Lett. 12 (2012) 1538–1544, https://doi.org/10.1021/nl2043612.
[21] H. Li, Q. Zhang, C.C.R. Yap, B.K. Tay, T.H.T. Edwin, A. Olivier, D. Baillargeat, From bulk to monolayer MoS_2: evolution of Raman scattering, Adv. Funct. Mater. 22 (2012) 1385–1390, https://doi.org/10.1002/adfm.201102111.
[22] B. Chakraborty, H.S.S.R. Matte, A.K. Sood, C.N.R. Rao, Layer-dependent resonant Raman scattering of a few layer MoS_2, J. Raman Spectrosc. 44 (2013) 92–96, https://doi.org/10.1002/jrs.4147.
[23] H.B. Michaelson, The work function of the elements and its periodicity, J. Appl. Phys. 48 (1977) 4729–4733, https://doi.org/10.1063/1.323539.
[24] S. Halas, T. Durakiewicz, Work functions of elements expressed in terms of the Fermi energy and the density of free electrons, J. Phys. Condens. Matter 10 (1998) 10815–10826, https://doi.org/10.1088/0953-8984/10/48/005.
[25] T. Drummond, Work functions of the transition metals and metal silicides, 1999, pp. 1–34, doi.org/ark:/67531/metadc681130.
[26] F. Wang, Z. Wang, Q. Wang, F. Wang, L. Yin, K. Xu, Y. Huang, J. He, Synthesis , properties and applications of 2D non-graphene materials, Nanotechnology 26 (2015) 292001, https://doi.org/10.1088/0957-4484/26/29/292001.
[27] K. Lee, H.-Y. Kim, M. Lotya, J.N. Coleman, G.-T. Kim, G.S. Duesberg, Electrical characteristics of molybdenum disulfide flakes produced by liquid exfoliation, Adv. Mater. 23 (2011) 4178–4182, https://doi.org/10.1002/adma.201101013.
[28] N. Kaushik, A. Nipane, F. Basheer, S. Dubey, S. Grover, M.M. Deshmukh, S. Lodha, Schottky barrier heights for Au and Pd contacts to MoS_2, Appl. Phys. Lett. 105 (2014) 1–5, https://doi.org/10.1063/1.4895767.
[29] F. Liu, W.L. Chow, X. He, P. Hu, S. Zheng, X. Wang, J. Zhou, Q. Fu, W. Fu, P. Yu, Q. Zeng, H.J. Fan, B.K. Tay, C. Kloc, Z. Liu, Van der Waals p–n junction based on an organic–inorganic heterostructure, Adv. Funct. Mater. 25 (2015) 5865–5871, https://doi.org/10.1002/adfm.201502316.
[30] V.L. Rideout, A review of the theory and technology for ohmic contacts to group III–V compound semiconductors, Solid State Electron. 18 (1975) 541–550, https://doi.org/10.1016/0038-1101(75)90031-3.
[31] P. Stallinga, Electrical characterization of organic electronic materials and devices. http://eu.wiley.com/WileyCDA/WileyTitle/productCd-047075009X.html, 2009.
[32] B. Roul, M. Kumar, M.K. Rajpalke, T.N. Bhat, S.B. Krupanidhi, Binary group III-nitride based heterostructures: band offsets and transport properties, J. Phys. D Appl. Phys. 48 (2015) 423001, https://doi.org/10.1088/0022-3727/48/42/423001.
[33] S. Averine, Y.C. Chan, Y.L. Lam, Evaluation of Schottky contact parameters in metal–semiconductor–metal photodiode structures, Appl. Phys. Lett. 77 (2000) 274–276, https://doi.org/10.1063/1.126948.
[34] P. Bampoulis, R. Van Bremen, Q. Yao, B. Poelsema, H.J.W. Zandvliet, K. Sotthewes, Defect dominated charge transport and fermi level pinning in MoS_2/metal contacts, ACS Appl. Mater. Interfaces 9 (2017) 19278–19286, https://doi.org/10.1021/acsami.7b02739.
[35] A.J. Chiquito, C.A. Amorim, O.M. Berengue, L.S. Araujo, E.P. Bernardo, E.R. Leite, Back-to-back Schottky diodes: the generalization of the diode theory in analysis and extraction of electrical parameters of nanodevices, J. Phys. Condens. Matter 24 (2012) 225303, https://doi.org/10.1088/0953-8984/24/22/225303.
[36] P. Vabbina, N. Choudhary, A.-A. Chowdhury, R. Sinha, M. Karabiyik, S. Das, W. Choi, N. Pala, Highly sensitive wide bandwidth photodetector based on internal photoemission in CVD grown p-type MoS_2/graphene Schottky junction, ACS Appl. Mater. Interfaces 7 (2015) 15206–15213, https://doi.org/10.1021/acsami.5b00887.
[37] J. Kang, W. Liu, D. Sarkar, D. Jena, K. Banerjee, Computational study of metal contacts to monolayer transition-metal dichalcogenide semiconductors, Phys. Rev. X. 4 (2014) 1–14, https://doi.org/10.1103/PhysRevX.4.031005.
[38] W. Wu, Y. Li, L. Liang, Q. Hao, J. Zhang, H. Liu, C. Liu, Enhanced broadband responsivity of Ni-doped Sb_2Se_3 nanorod photodetector, J. Phys. Chem. C 123 (2019) 14781–14789, https://doi.org/10.1021/acs.jpcc.9b02320.
[39] G.M. Ali, P. Chakrabarti, ZnO-based interdigitated MSM and MISIM ultraviolet photodetectors, J. Phys. D Appl. Phys. 43 (2010) 415103, https://doi.org/10.1088/0022-3727/43/41/415103.
[40] A. Islam, J. Lee, P.X.-L. Feng, Atomic layer GaSe/MoS_2 van der Waals heterostructure photodiodes with low noise and large dynamic range, ACS Photonics 5 (2018) 2693–2700, https://doi.org/10.1021/acsphotonics.8b00318.
[41] F. Yu, M. Hu, F. Kang, R. Lv, Flexible photodetector based on large-area few-layer MoS_2, Prog. Nat. Sci. Mater. Int. 28 (2018) 563–568, https://doi.org/10.1016/j.pnsc.2018.08.007.
[42] P.R. Berger, Metal-semiconductor-metal photodetectors, Proc. SPIE-Int. Soc. Opt. Eng. 4285 (2001) 198–207, https://doi.org/10.1117/12.426888.
[43] L. Dong, J. Yu, R. Jia, J. Hu, Y. Zhang, J. Sun, Self-powered MSM deep-ultraviolet B-Ga_2O_3 photodetector realized by an asymmetrical pair of Schottky contacts, Opt. Mater. Express 9 (2019) 1191–1199, https://doi.org/10.1364/OME.9.001191.
[44] Z.L. Wang, Progress in piezotronics and piezo-phototronics, Adv. Mater. 24 (2012) 4632–4646, https://doi.org/10.1002/adma.201104365.
[45] H.-Y. Chen, K.-W. Liu, X. Chen, Z.-Z. Zhang, M.-M. Fan, M.-M. Jiang, X.-H. Xie, H.-F. Zhao, D.-Z. Shen, Realization of a self-powered ZnO MSM UV photodetector with high responsivity using an asymmetric pair of Au electrodes, J. Mater. Chem. C. 2 (2014) 9689–9694, https://doi.org/10.1039/C4TC01839G.
[46] A. Di Bartolomeo, G. Luongo, F. Giubileo, N. Funicello, G. Niu, T. Schroeder, M. Lisker, G. Lupina, Hybrid graphene/silicon Schottky photodiode with intrinsic gating effect, 2D Mater. 4 (2017) 25075, https://doi.org/10.1088/2053-1583/aa6aa0.
[47] J. Woo, H. Hwang, Communication—comprehensive assessment of a back-to-back Schottky diode with ultrathin TiO_2 layer for cross-point selector applications, ECS J. Solid State Sci. Technol. 5 (2016) Q188–Q190, https://doi.org/10.1149/2.0301606jss.
[48] J. Quereda, T.S. Ghiasi, F.A. van Zwol, C.H. van der Wal, B.J. van Wees, Observation of bright and dark exciton transitions in monolayer $MoSe_2$ by photocurrent spectroscopy, 2D Mater. 5 (2017) 15004, https://doi.org/10.1088/2053-1583/aa8aa0.
[49] K.K. Kam, B.A. Parkinson, Detailed photocurrent spectroscopy of the semiconducting group VIB transition metal dichalcogenides, J. Phys. Chem. 86 (1982) 463–467, https://doi.org/10.1021/j100393a010.